13 (2022) 100081

Contents lists available at ScienceDirect

Journal of Non-Crystalline Solids: X

journal homepage: www.sciencedirect.com/journal/journal-of-non-crystalline-solids-x

Decompression dynamics of high density amorphous ice above and below the liquid-liquid critical point

Edoardo Maria Mollica [a], John Russo [a], H. Eugene Stanley [b], Francesco Sciortino [a,*]

[a] Department of Physics, Sapienza University of Rome, Italy
[b] Boston University, Center for Polymer Science, Boston, MA, USA

ARTICLE INFO

Keywords:
Supercooled water
Amorphous ice
Phase transition
Computer simulation

ABSTRACT

We investigate via numerical simulations of the TIP4P/Ice model the isothermal decompression of high density amorphous ice (HDA) mirroring the experimental protocol followed by recent experiments [H. K. Kim, et al., Science **370**, 978, 2020]. Taking advantage of the recent determination of the TIP4P/Ice liquid-liquid critical point, we decompress our samples at temperatures both below and above the critical temperature. We follow the crossover between high and low density, complementing the time evolution of the structure factor with the time evolution of microscopic descriptors. Our results support the interpretation of the experimental pathway as a structural change from high to low density states through a first-order transition line. In the simulation study we do not observe nucleation events, but rather a spinodal-like non-equilibrium transformation, which offers an explanation on why the decompression process even at sub-critical temperatures may result in a continuous time evolution of the density and of the microscopic descriptors.

Nearly 30 years ago, Poole et al. [1], proposed to explain the growth of water's response functions on cooling invoking the presence of a liquid-liquid critical point (LLCP) located in a temperature-pressure region where the liquid phase is metastable with respect to ice. According to this hypothesis, a transition line exists in supercooled liquid water, separating two liquid phases: a high density (HDL) and a low density liquid (LDL). The idea that the same molecule can form two distinct disordered condensed phases, considered an exotic possibility when first proposed, is now regarded as the most probable scenario for describing the behavior of water.

The original results based on the ST2 model [2], despite the limited size and computational time, have been confirmed by studies based on significantly more powerful computational resources [3,4] and algorithmic developments [5–8]. Very recently the critical fluctuations, first observed in the ST2 model, have also been found simulating water with more accurate classical potential models [9].

A natural connection to the LLCP scenario is found in two-state models of water [10–13], which posit that local configurations in liquid water can be grouped in two states that correspond to low density (LD) and high density (HD) environments respectively. Numerical [14–20] and experimental [21–27] evidence of two-state behavior in water points to a possible critical demixing of the two-states in deeply supercooled state [28].

Strong support toward the existence of the LLCP is also provided by the existence of two distinct glasses, differing in density and structure [29] in a way strongly reminiscent of the expected difference between the two liquid phases [30,31]. From an experimental point of view, the observed first-order like transition between these two amorphous forms on varying pressure [32,33], the evidence of two different calorimetric glass transitions [34], and the distinct heating profiles of the two glasses [35] are all consistent with the LLCP prediction. A direct thermodynamic link between two glasses (LDA and HDA) and two liquids (LDL and HDL) has recently been proposed via a neural network analysis of local environments [36]. Recent experiments have also confirmed the connection between the amorphous ices and the liquids by investigating vitrified droplets [37].

Experimental studies of water anomalies have also significantly restricted the number of possible alternative thermodynamic scenarios. Examples include the recently measured behavior of stretched water [38], and the maxima at ambient pressure in the compressibility [39] and in the specific heat [40].

In 2020 A. Nilsson and collaborators reported experimental findings that directly probe the cross-over from high to low density liquid [41]. They applied an ultrafast heating beam to a high-density amorphous

* Corresponding author.
E-mail address: francesco.sciortino@uniroma1.it (F. Sciortino).

https://doi.org/10.1016/j.nocx.2022.100081
Received 14 November 2021; Received in revised form 6 January 2022; Accepted 9 January 2022
Available online 12 January 2022

sample, bringing the sample in the no-mans land, then following the time evolution of the local structure via X-ray scattering. In the experiment, the authors have been able to follow the transition from the high to the low density liquid on the microsecond time scale, confirming that the liquid-liquid transition takes place just before ice nucleation occurs in the sample.

Here we perform molecular dynamics simulations designed to reproduce in silico the out-of-equilibrium pathway of the experiment by H. K. Kim et al. [41]. Very recently, a simulation study aimed at reproducing the same experiment was presented in Ref. [42], where the ST2 water model was chosen and the isothermal decompression is performed with a barostat with a rate approximately 100 times faster than that of the experiments. In our simulations we use the TIP4P/Ice water model, and prepare the system in a slab geometry to decompress the HDA sample without the need of a barostat. Due to numerical limits, the width of the slab is significantly smaller than the experimental one and the possible consequences of this smaller size should be investigated in detail in future studies. Apart from this difference, the numerical investigation attempts to reproduce as close as possible the experimental set-up. We perform the same analysis used in the experiments. In addition, we complement them with the time dependence of microscopic descriptors, providing a detailed molecular scale description of the transformation process.

1. The experiment in silico

In the experiment of Ref. [41], a layer of $(30 \div 50)$ μm thick high-density glass sample is irradiated by a ultra-fast infrared (IR) laser pulse ($\sim$100 fs, 2 μm) that increases instantaneously and isochorically the vibrational temperature of the sample. The temperature jump produced by the IR heating brings the temperature of the slab around 205 ± 10 K, as estimated in the experiment from temperature-induced shifts in the Bragg reflections. The sample is then left to equilibrate at ambient pressure and the associated relaxation kinetics is recorded by an X-ray laser pulse ($\sim$50 fs, 9.7 Kev) at various time intervals (covering tens of microseconds), until crystallization arises. During the relaxation, the sample density progressively decreases with a negligible temperature variation (isothermal decompression).

We model the water-water interaction using the `TIP4P/Ice` model [43], a rigid model optimized to reproduce the behavior of supercooled water. The choice of the water model is motivated by the recent determination of its liquid-liquid critical point at $T = 188.6$ K and $P = 1725$ bar [9]. The simulations are carried out using `GROMACS 5.1.4` [44] with a leapfrog algorithm with a time step of 2 fs, using a `Nose-Hover` thermostat.

The first step of our simulation protocol is the preparation of samples of HDA glass. This is obtained by simulating a high density liquid configuration for $\approx 23\,\mu$s at $T = 160$ K and $P = 2500$ bar or higher (i.e. in the HDL region of the phase diagram). The shape of the simulation box, containing $N = 3000$ water molecules, is a rectangular cuboid with a $3 \times 1 \times 1$ ratio and periodic boundary conditions. The last configuration of the $T = 160$ K run is quenched, preserving the volume, at $T = 77$ K to generate the HDA phase. Then, in agreement with the experimental protocol, the HDA configuration is recovered at ambient pressure, always at $T = 77$ K. The average density at this point is 1.118 ± 0.007 g/cm^3. In order to reproduce the geometry of the experimental setup, the second step of our protocol involves the creation of a 9 nm slab of HDA glass. We first expand the box size along the x direction to 200 nm, effectively creating an interface with vacuum (but without observing evaporation of any molecule from the surface). The large length of the box along x is chosen in order to avoid any interactions between the repeating images of the molecules along the x direction. A short equilibration ($\approx 0.3\,\mu$s) at ambient pressure and $T = 77$ K is then performed to allow local rearrangements of the molecules located on the surface. Fig. 1 shows a pictorial representation of the simulation setup.

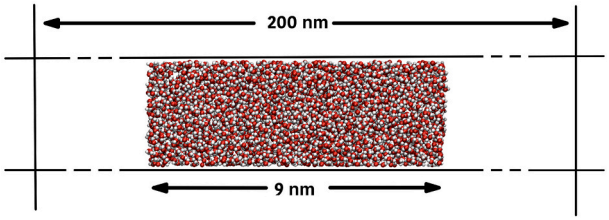

Fig. 1. Orthogonal projection along the x and y axis of the simulation box. The slab thickness is $\approx$9 nm, while the whole box spans for 200 nm in lenght, hence creating the interface with vacuum. Along the y and z axis ($\approx$3 nm long), periodic boundary conditions are imposed.

As previously alluded, the width of the slab in the simulation ($\approx$9 nm) is significantly smaller than the experimental one (30–50 μm). We cannot exclude that this limited size affects the relaxation times (for example by coupling of elastic and diffusive processes). The present contribution must thus be considered as a first attempt to investigate the decompression dynamics of a high density liquid mimicking as close as possible the experimental protocol. Further investigations, focusing on the slab-size effect (as well as on the dependence of the results on the preparation of the high-density glass) will be required for a definitive validation of the present results.

The IR laser heating was simulated rescaling the velocities to the desired final temperature T, followed by a coupling to a `Nose-Hoover` thermostat with characteristic times $\tau_T = 1.87$ ps providing a fast thermalization of the vibrational degrees of freedom. We investigated several T values, specifically $T = 160$ K, $T = 170$ K, $T = 180$ K, $T = 185$ K, $T = 192$ K.

To follow the kinetic associated with the transition from the high density configuration to the low density one, we analysed only the central part of the slab (of approximately width of 3 nm). This inner part of the configuration is significantly separated (by 3 nm on each side) by the slab boundaries and hence it can be considered as a representation of the bulk behavior of the system. All quantities that follow refer only to the molecules in the central slab.

Being an out-of-equilibrium process, where only the kinetic temperature and the density are properly defined, it is not possible to unambiguously draw a transformation pathway on the phase diagram. Still, one can correlate the starting density with the known equilibrium equation of state [20] to draw approximately the starting and ending points of the transformation on the (P, T) plane, as shown in Fig. 2 for the simulations at $T = 180$ K and at $T = 192$ K. Note that the $T = 180$ K $< T_C$ path crosses the liquid-liquid transition line, while the other path at $T > T_C$ (i.e. $T = 192$ K) lies entirely in the supercritical region.

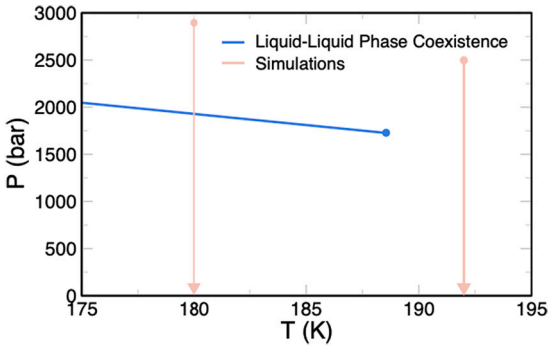

Fig. 2. (P, T) phase diagram of the TIP4P/Ice model showing the LLCP (blue circle) and the liquid-liquid transition line (blue). Also shown (pink lines) are the isothermal decompression paths at two of the studied temperatures, $T = 180$ K and at $T = 192$ K.

2. Results

Fig. 3 shows the time evolution of the density during the equilibration process. Following the very fast expansion associated to the thermalization of the vibrational degrees of freedom at T, the density slowly evolves toward the $\rho \approx 0.95$ g/cm^3 value expected for this model at ambient pressure [20]. We observe a continuous change from a density value characteristic of the high density liquid to a value characteristic of the low density liquid. Even at temperatures below T_c, where the path crosses the equilibrium location of the liquid-liquid transition, the density change progresses with continuity (no clear signature of a plateau or a change in concavity), suggesting the absence of nucleation events.

The oxygen-oxygen radial distribution function $g(\mathbf{r})$ (evaluated only for molecules belonging to a 3 nm thick slab equidistant from the interfaces) highlights the major changes in local structure taking place during the process and it is plotted in Fig. 4a. Specifically, the signature of the interstitial molecules in the region between the first and the second shell of the molecules ($r \approx 0.35$ nm), a characteristic of the high density liquid (and glass), progressively disappears, signalling the formation of local configurations in which water's tetrahedral geometry is recognisable [31,45].

To make contact with the experiments, we evaluate by Fourier transform of $g(r)$ the oxygen-oxygen structure factor $S(q)$, and plot it in Fig. 4b. The figure shows the progressive shift of the first diffraction peak from $q_{HD} \approx 21$ nm^{-1} to $q_{LD} \approx 17$ nm^{-1}, the same peak position observed in the HDA and LDA ices [34]. The position of this pre-peak is considered a signature of the dominant locally favored structure [46]. Differently from what has been observed experimentally in the transformation from eHDA and LDA [34], we do not observe a time at which the $S(q)$ has a double peak shape. It has been suggested that the double peak structure could be masked by interference effect between low and high density regions when the correlation length of these region is of the order of a few molecular diameters. Further work could clarify if this difference is a genuine feature or if it arises from the finite size of the studied system.

2.1. Spectral decomposition

Here we analyze the structure factor $S(q)$ following a protocol similar to the one applied in the experimental study, fitting the time evolution of $S(q)$ in the region of the pre-peak (15 nm^{-1} < q < 25 nm^{-1}) and the following two peaks (q < 60 nm^{-1}) with the sum of two Gaussians and two Lorentzians

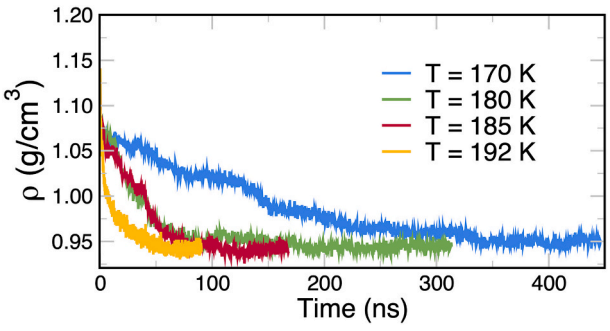

Fig. 3. Density evolution during aging for the simulations at: $T = 170$ K (*blue*), $T = 180$ K (*green*), $T = 185$ K (*red*), $T = 192$ K (*yellow*). (For interpretation of the references to colour in this figure legend, the reader is referred to the web version of this article.)

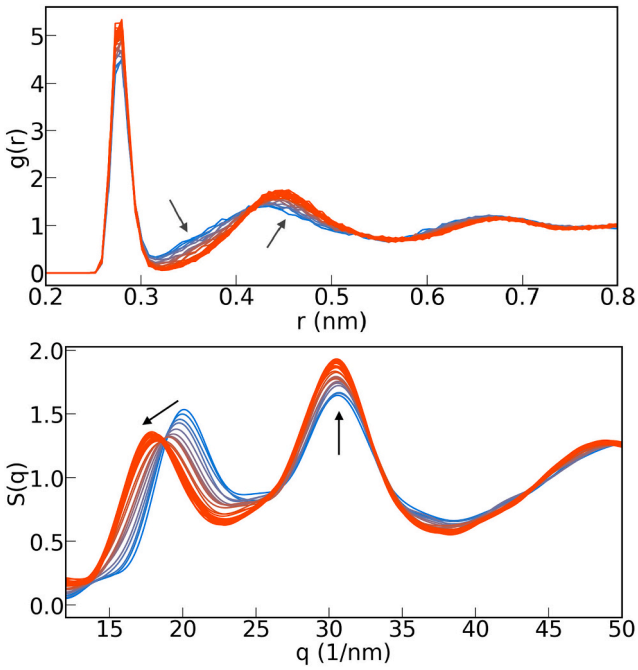

Fig. 4. Structural changes occurring during the relaxation of the $T = 180$ K simulation. The colour change represents time (from blue to red) and each line is taken at intervals of ≈5 ns apart. The oxygen-oxygen pair correlation function (*top panel)* shows a gradual decrease in the interstitial region ($r \approx 0.35$ nm) n while the corresponding structure factor (*bottom panel*) shows the change in the pre-peak position. The arrows indicates the time evolution. (For interpretation of the references to colour in this figure legend, the reader is referred to the web version of this article.)

$$S(q) = \frac{a_{LD}}{\pi}\frac{\Gamma_{\mathrm{LD}}}{(q-q_{LD})^2-\Gamma_{LD}^2} + \frac{a_{HD}}{\sqrt{2\pi\sigma_{HD}^2}}e^{-\frac{(q-q_{HD})^2}{2\sigma_{HD}^2}} + \\ + \frac{a_{T3}}{\pi}\frac{\Gamma_{\mathrm{T3}}}{(q-q_{T3})^2-\Gamma_{T3}^2} + \frac{a_{T4}}{\sqrt{2\pi\sigma_{T4}^2}}e^{-\frac{(q-q_{T4})^2}{2\sigma_{T4}^2}} \quad (1)$$

where the coefficient a_i, Γ_i, q_i, σ_i for $i = HD, LD, T3, T4$ are the free parameters of the fit. This functional form has been proposed by Shi and Tanaka [46] to quantify the role of low and high local density regions in supercooled water. In this functional form, the first Lorentzian, centered in q_{LD}, captures the contribution of the tetrahedrally coordinated molecules while the first Gaussian, centred at q_{HD} captures the contribution from molecules in a local higher density configuration. The additional Lorentzian and Gaussian contribution in Eq. (1) (centred at q > 30 nm^{-1}) are added to capture the leakage of the two successive peaks in the selected window. The integrated area below the first two contributions provides a quantification of the fraction of molecules in low and high density environments respectively. Fig. 5 shows the least squares fit and the evolution of the two contributions during the relaxation of the sample. We note that, differently from Ref. [41], where an HD, LD and crystalline peak were used to fit the pre-peak in $S(q)$, here we do not account for a crystalline contribution, as homogeneous nucleation does not occur in the time scale of the simulations. In agreement with the results in Ref. [41], Fig. 5 shows how the HD contribution is converted into its lower density counterpart LD. The populations extracted from the fits will be discussed in conjunction with other microscopic descriptors in the following.

2.2. Microscopic descriptors

Here we provide a microscopic description of the system evolution

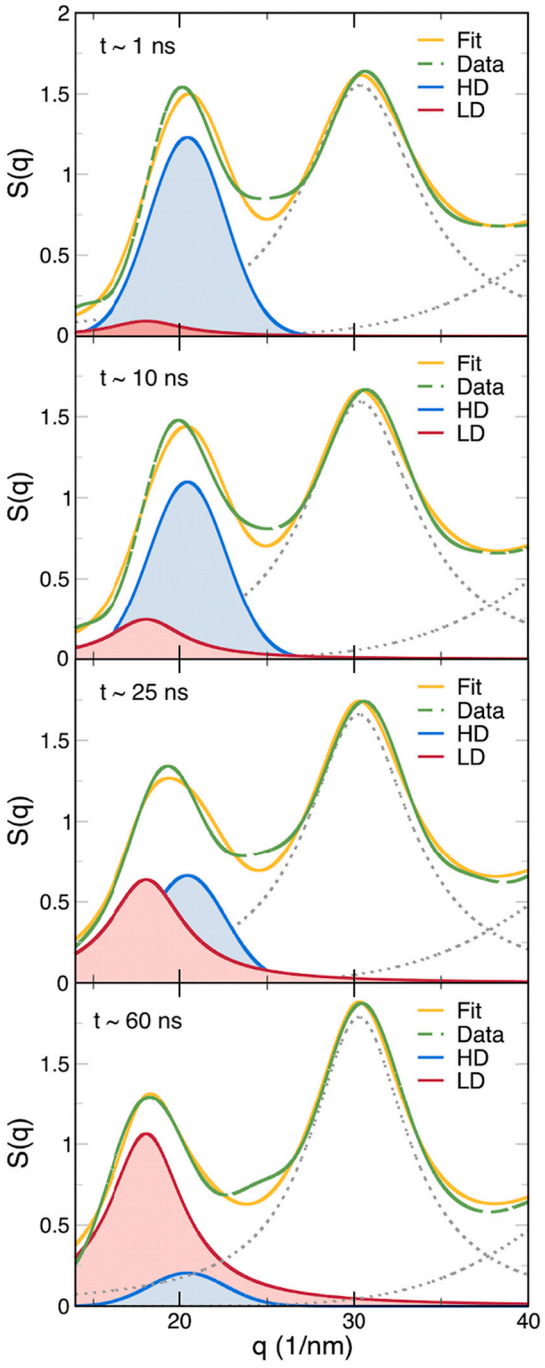

Fig. 5. Oxygen-Oxygen structure factor $S(q)$ — calculated by Fourier transform of the $g(r)$ — of the $T = 180$ K simulation during the decompression process (*green dashed*). The *yellow* curves indicate the fit according to Eq. (1). The $S(q)$ pre-peak is fitted by the sum of the blue Gaussian (HD) and the red Lorentzian (LD). The dotted components are used to fit the rest of the data. The graph shows the evolution of the peak position during the decompression from short (*top*) to long times (*bottom*). (For interpretation of the references to colour in this figure legend, the reader is referred to the web version of this article.)

extracted from the numerical trajectories. We focus on two descriptors which have been proposed in the past to identify the local structure of each individual water molecule. Specifically we focus on d_5 [47] and ζ [15]. d_5 is defined as the distance of the fifth oxygen atom from the selected molecule. ζ requires also information on the hydrogen bonded neighbours of the selected molecule. It expresses the distance between the second and first shell. ζ [15] has been shown to successfully capture the anomalous contribution to water anomalies over a large range of temperatures and pressures [15,48]. For a review of other methods for local structure determination in water see Ref. [49].

The distribution of both descriptors for different times during the relaxation of the sample are plotted in Fig. 6. Both descriptors are characterized by a broad distribution of values which progressively shifts to larger values with time and a non-monotonous evolution of the height of the distribution. The value of the descriptor corresponding to the peak position of the minimum height of the distribution (which represents equimolar mixing) is used as a threshold ($d_5 = 0.36$ and $\zeta = 0.75$) to separate molecules in either a high-density (HD) or low-density (LD) environment, for values lower or higher than the threshold respectively. With this procedure, initially most of the molecules are described by the HD type while at the end of the simulation most of the molecule are classified as LD. As for the analysis of the structure factor, the time evolution of the number of HD molecules (or equivalently of the LD type) provides a quantification of the time dependence of the local structural changes.

Fig. 7 compares the time evolution of the LD populations extracted from the fit of the structure factor (top panel), and the structural descriptors ζ (middle panel) and d_5 (bottom panel). For each quantity we plot the relaxation at temperatures below ($T = 170$ K, $T = 180$ K) and above ($T = 192$ K) the critical temperature of $T_c = 188.6$ K. The different quantities show a similar relaxation dynamics, with the population of low density environments going from the minority at $t = 0$ to the majority component on similar timescales. This timescale depends on the temperature, with the higher temperature relaxing faster. The same trend is observed for samples prepared at different initial densities and for different quenching temperatures (not shown). We also observed that the appearance of the low density population does not take place in a well defined region of the sample, but it is distributed homogeneously over the entire volume, confirming the absence of nucleation phenomena, both below and above T_c.

Comparing our results to the experiments of Ref. [41], we note that

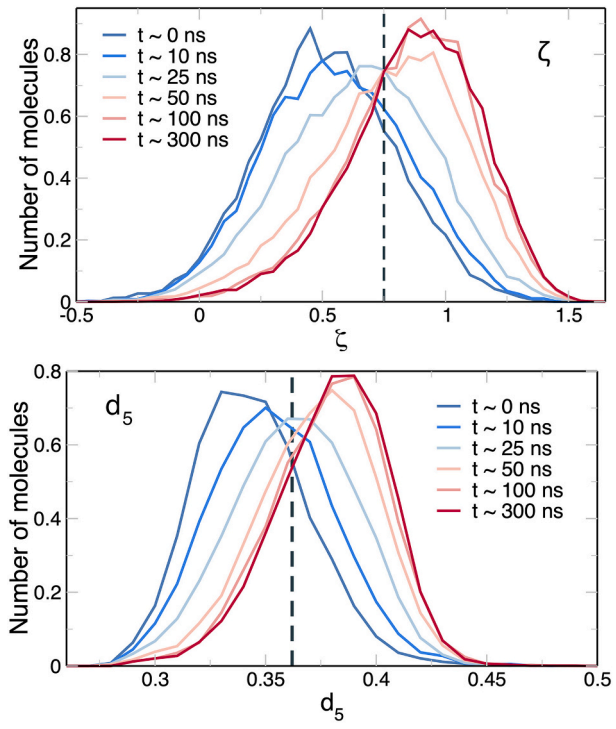

Fig. 6. Histograms showing the distribution of the d_5 (*bottom*) and the ζ (*top*) structural indicators during the decompression process. The dashed black line represents the selected threshold to distinguish between low and high density populations. Here $T = 180$ K.

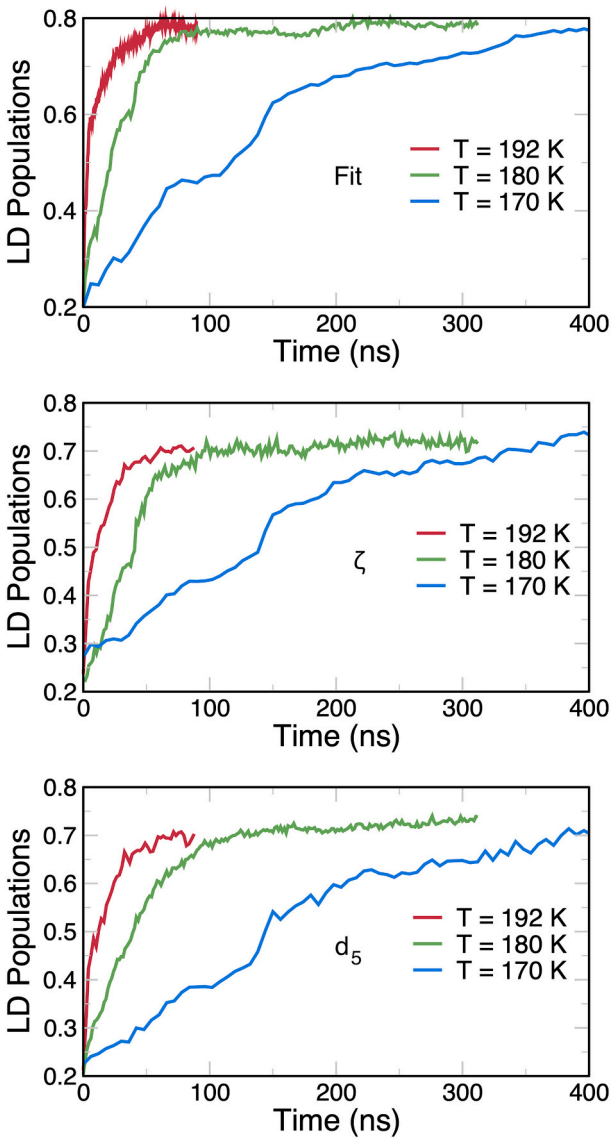

Fig. 7. Evolution of the low density population during decompression resulting from the fit of $S(q)$ (*top panel*), from the ζ descriptor (*middle panel*) and from the d_5 descriptor (*bottom panel*) for simulations above ($T = 192$ K) and below ($T = 180$ K, $T = 170$ K) the critical temperature T_C.

while in the experiments the LDL component reaches a 40% fraction on a timescales of ≈ 1 μs, the simulations display T-dependent dynamics that appear to be faster compared with the experimental timescale. Independently on the value of T we observe similar relaxation pathways. The comparison between the evolution of the structure factor and the microscopic descriptors allows us to confirm the interpretation of the relaxation process observed in the evolution of the structure factor as originating from the interconversion between HD and LD populations. Our results thus support the interpretation provided in the experimental study [41] in term of interconversion between two liquid-phases at $T < T_c$. No clear distinction in the relaxation pathway is observed for trajectories with $T > T_c$ via the descriptors of Fig. 7, making the analysis insensitive to the location of the critical point.

3. Discussions and conclusion

In summary, we have performed simulations of the TIP4P/Ice model with the goal of reproducing the decompression pathway of HDA observed in the experiments of Ref. [41], qualitatively duplicating the experimental observations. More precisely we have observed a similar time evolution of the structure factor's pre-peak, which continuously changes from a shape typical of the high density amorphous ice to a shape typical of the low density amorphous ice. While this change is fully compatible with two-state model predictions [46], the inherently out-of-equilibrium nature of the transformation does not allow to definitively locate the presence of a corresponding equilibrium liquid-liquid critical point (notwithstanding TIP4P-Ice has one). Despite their intrinsic limitations (constraints on time and length scales, and the use of simplified potentials), simulations offer important insights into the studied kinetic process. First, by analyzing the simulation trajectories, we unambiguously attribute the shift of the structure factor's pre-peak to a change of local environments from high to low density. Second, the numerical results are not affected by crystallization. Finally, differently from the experiments, we know exactly the location of the liquid-liquid critical point and are able to compare the decompression dynamics both above and below the critical temperature. Our choice of the TIP4P-Ice model was indeed motivated by the recent determination of its critical parameters [9].

The results show that the change in the structure factor's pre-peak are not sufficient to distinguish the relative distance from the critical point. Even for $T < T_c$ no clear signatures of activated processes (expected in a nucleation event) have been observed. We stress that at the present time we cannot rule out the possibility that finite size effects (the slab width) can significantly alter the observed relaxation pathway. We cannot also exclude a dependence originating from the protocol chosen to build the starting high-density glass configuration. Finally, effects arising from the different molecular mobility of the TIP4P-Ice model as compared to water cannot be excluded. Future studies must definitively address these possibilities. Despite these uncertainties, we propose here a thermodynamic-based possible explanation of the reasons why nucleation phenomena has not been observed. Fig. 8, shows a schematic equation of state (EOS) for the case in which a LL transition exists. The figure indicates a starting state in the high density branch of the EOS and two possible final states, one inside the liquid-liquid coexistence region (left panel) and one at much lower pressure (right panel), mimicking the ambient pressure conditions of the experiment and of the present simulation. In the first case (path a), assuming a path composed of quasi-equilibrium states, upon expansion the density will follow the HD branch and then undergo nucleation to cross the free-energy barrier that separates it from the the LD branch. In the second case (path b), the density will still follow the HD branch down to minimum in the EOS, and will then proceed, in the absence of any thermodynamic barrier, toward

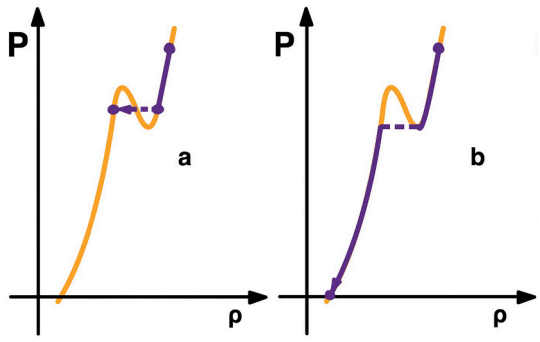

Fig. 8. Schematic representation of the EOS for supercooled water. The hypothesised Liquid-Liquid transition is depicted by the Van der Waals (VdW) loop. The left graph (a) represents a path with a final pressure inside the metastable region of the VdW loop. In this case, the system evolves toward the final equilibrium state undergoing nucleation. The right graph (b) represents the path along the EOS for a quench to $P = 0$ bar, visualizing the case in which the pressure is smaller than the pressure values in the VdW loop. In this case the system does not need to overcome any free energy barrier to evolve toward equilibrium.

the low density case. Indeed, in mean field, the height of the barrier at the minimum vanishes. This qualitative explanation is consistent with the transformation of molecules from HD to LD over all the simulated samples and the absence of a plateau in the time evolution of the density [50,51].

Finally, we stress that a quench from high to ambient pressure at $T > T_c$ would produce a similarly smooth density evolution, in agreement with the results reported in Fig. 7. Only in the very low wavevector range, outside the window explored in both experiments and simulations, differences between under-critical ($T < T_c$) and super-critical ($T > T_c$) paths could possibly be observed.

The simulation results presented in this article thus corroborate the experimental study of Ref. [41], confirming the clear cross-over from high-density to low-density local order, well before crystallization takes place. Differently from standard nucleation events, we do not observe a plateau followed by a steep variation in the time evolution of the density and of the structural indicators either evaluated from a two-population analysis of the structure factor or from microscopic local order parameters such as d_5 and ζ.

We stress that the absence of a clear nucleation and growth of the low density phase is consistent with a quench to pressures smaller than the values for which the van der Waals loop exists (see Fig. 7(b)), a path that (in mean field) does not encounter any thermodynamic barrier. Hence, the standard signatures of a first-order transition (a fast equilibration to the original phase followed — at a random time — by one or more nucleation events generating critical nuclei of the stable phase, further followed by their growth) should not be expected. Finally we observe that, the time dependence of the structural indicators is not significantly different below and above T_c. In this respect, the study of decompression protocols near the critical point will require future investigation in the low-q region.

Declaration of Competing Interest

The authors declare that they have no known competing financial interests or personal relationships that could have appeared to influence the work reported in this paper.

Acknowledgements

This work is dedicated to the memory of C. Austen Angell, who we hold dear both as much as a scientist and as a friend. His love for the physics of supercooled water has deeply affected us. JR acknowledges support from the European Research Council Grant DLV-759187. FS acknowledges support from Ministero dell'Istruzione, dell'Università e della Ricerca (MIUR) Progetti di Ricerca d'Interesse Nazionale (PRIN) 2017 (Project 2017Z55KCW) and HPC-CINECA for providing computational resources. We thank N. Giovambattista, A. Nilsson and P. Poole for constructive comments on the first draft of this work.

References

[1] P.H. Poole, F. Sciortino, U. Essmann, H.E. Stanley, Phase behaviour of metastable water, Nature 360 (1992), https://doi.org/10.1038/360324a0.
[2] P.H. Poole, F. Sciortino, U. Essmann, H.E. Stanley, Spinodal of liquid water, Phys. Rev. E 48 (1993) 3799–3817, https://doi.org/10.1103/PhysRevE.48.3799. URL https://link.aps.org/doi/10.1103/PhysRevE.48.3799.
[3] P.H. Poole, I. Saika-Voivod, F. Sciortino, Density minimum and liquid–liquid phase transition, J. Phys. Condens. Matter 17 (43) (2005) L431–L437, https://doi.org/10.1088/0953-8984/17/43/l01.
[4] T.A. Kesselring, G. Franzese, S.V. Buldyrev, H.J. Herrmann, H.E. Stanley, Nanoscale dynamics of phase flipping in water near its hypothesized liquid-liquid critical point, Sci. Rep. 2 (1) (2012) 1–6.
[5] Y. Liu, A.Z. Panagiotopoulos, P.G. Debenedetti, Low-temperature fluid-phase behavior of st2 water, J. Chem. Phys. 131 (10) (2009), 104508.
[6] F. Sciortino, I. Saika-Voivod, P.H. Poole, Study of the st2 model of water close to the liquid–liquid critical point, Phys. Chem. Chem. Phys. 13 (44) (2011) 19759–19764.
[7] P.H. Poole, R.K. Bowles, I. Saika-Voivod, F. Sciortino, Free energy surface of st2 water near the liquid-liquid phase transition, J. Chem. Phys. 138 (3) (2013), 034505.
[8] J.C. Palmer, F. Martelli, Y. Liu, R. Car, A.Z. Panagiotopoulos, P.G. Debenedetti, Metastable liquid–liquid transition in a molecular model of water, Nature 510 (7505) (2014) 385–388.
[9] P.G. Debenedetti, F. Sciortino, G.H. Zerze, Second critical point in two realistic models of water, Science 369 (2020), https://doi.org/10.1126/science.abb9796.
[10] C.T. Moynihan, Two species/nonideal solution model for amorphous/amorphous phase transitions, MRS Online Proc. Library Archive 455 (1996).
[11] M.A. Anisimov, M. Duška, F. Caupin, L.E. Amrhein, A. Rosenbaum, R.J. Sadus, Thermodynamics of fluid polyamorphism, Phys. Rev. X 8 (1) (2018), 011004.
[12] H. Tanaka, Liquid–liquid transition and polyamorphism, J. Chem. Phys. 153 (13, 2020) 130901.
[13] F. Caupin, M.A. Anisimov, Minimal microscopic model for liquid polyamorphism and waterlike anomalies, Phys. Rev. Lett. 127 (2021), 185701.
[14] M.J. Cuthbertson, P.H. Poole, Mixturelike behavior near a liquid-liquid phase transition in simulations of supercooled water, Phys. Rev. Lett. 106 (11, 2011) 115706.
[15] J. Russo, H. Tanaka, Understanding water's anomalies with locally favoured structures, Nat. Commun. 5 (1) (2014) 1–11.
[16] R. Shi, J. Russo, H. Tanaka, Common microscopic structural origin for water's thermodynamic and dynamic anomalies, J. Chem. Phys. 149 (22, 2018) 224502.
[17] F. Martelli, Unravelling the contribution of local structures to the anomalies of water: the synergistic action of several factors, J. Chem. Phys. 150 (2019), 094506.
[18] J.M.M. de Oca, F. Sciortino, G.A. Appignanesi, A structural indicator for water built upon potential energy considerations, J. Chem. Phys. 152 (24, 2020) 244503.
[19] J.W. Biddle, R.S. Singh, E.M. Sparano, F. Ricci, M.A. González, C. Valeriani, J. L. Abascal, P.G. Debenedetti, M.A. Anisimov, F. Caupin, Two-structure thermodynamics for the tip 4p/2005 model of water covering supercooled and deeply stretched regions, J. Chem. Phys. 146 (3) (2017), 034502.
[20] R. Foffi, J. Russo, F. Sciortino, Structural and topological changes across the liquid-liquid transition in water, J. Chem. Phys. 154 (18) (2021) 184506. arXiv:2104.10144. https://doi.org/10.1063/5.0049299.
[21] V. Holten, M.A. Anisimov, Entropy-driven liquid–liquid separation in supercooled water, Sci. Rep. 2 (1) (2012) 1–7.
[22] A. Nilsson, C. Huang, L.G. Pettersson, Fluctuations in ambient water, J. Mol. Liq. 176 (2012) 2–16.
[23] A. Taschin, P. Bartolini, R. Eramo, R. Righini, R. Torre, Evidence of two distinct local structures of water from ambient to supercooled conditions, Nat. Commun. 4 (1) (2013) 1–8.
[24] R. Shi, H. Tanaka, Direct evidence in the scattering function for the coexistence of two types of local structures in liquid water, J. Am. Chem. Soc. 142 (6) (2020) 2868–2875.
[25] S. Woutersen, B. Ensing, M. Hilbers, Z. Zhao, C.A. Angell, A liquid-liquid transition in supercooled aqueous solution related to the hda-lda transition, Science 359 (6380) (2018) 1127–1131.
[26] L.G. Pettersson, Y. Harada, A. Nilsson, Do x-ray spectroscopies provide evidence for continuous distribution models of water at ambient conditions? Proc. Nat. Acad. Sci. 116 (35, 2019) 17156–17157.
[27] L. Kringle, W.A. Thornley, B.D. Kay, G.A. Kimmel, Reversible structural transformations in supercooled liquid water from 135 to 245 k, Science 369 (6510) (2020) 1490–1492.
[28] R. Shi, H. Tanaka, The anomalies and criticality of liquid water, Proc. Nat. Acad. Sci. 117 (43) (2020) 26591–26599.
[29] P.H. Handle, T. Loerting, F. Sciortino, Supercooled and glassy water: metastable liquid (s), amorphous solid (s), and a no-man's land, Proc. Nat. Acad. Sci. 114 (51) (2017) 13336–13344.
[30] N. Giovambattista, F.W. Starr, P.H. Poole, State variables for glasses: the case of amorphous ice, J. Chem. Phys. 150 (22, 2019) 224502.
[31] R. Foffi, F. Sciortino, Structure of high-pressure supercooled and glassy water, Phys. Rev. Lett. 127 (2021) 175502, https://doi.org/10.1103/PhysRevLett.127.175502. URL https://link.aps.org/doi/10.1103/PhysRevLett.127.175502.
[32] O. Mishima, L.D. Calvert, E. Whalley, 'Melting ice' i at 77 k and 10 kbar: a new method of making amorphous solids, Nature 310 (1984), https://doi.org/10.1038/310393a0.
[33] O. Mishima, L. Calvert, E. Whalley, An apparently first-order transition between two amorphous phases of ice induced by pressure, Nature 314 (6006) (1985) 76–78.
[34] F. Perakis, K. Amann-Winkel, F. Lehmkühler, M. Sprung, D. Mariedahl, J. A. Sellberg, H. Pathak, A. Späh, F. Cavalca, D. Schlesinger, A. Ricci, A. Jain, B. Massani, F. Aubree, C.J. Benmore, T. Loerting, G. Grübel, L.G.M. Pettersson, A. Nilsson, Diffusive dynamics during the high-to-low density transition in amorphous ice, Proc. Nat. Acad. Sci. 114 (2017) 8193–8198, https://doi.org/10.1073/pnas.1705303114. URL https://www.pnas.org/content/114/31/8193.
[35] K. Amann-Winkel, C. Gainaru, P.H. Handle, M. Seidl, H. Nelson, R. Böhmer, T. Loerting, Water's second glass transition, Proc. Nat. Acad. Sci. 110 (44) (2013) 17720–17725.
[36] F. Martelli, F. Leoni, F. Sciortino, J. Russo, Connection between liquid and non-crystalline solid phases in water, J. Chem. Phys. 153 (10, 2020) 104503.
[37] J. Bachler, J. Giebelmann, T. Loerting, Experimental evidence for glass polymorphism in vitrified water droplets, Proc. Nat. Acad. Sci. 118 (30) (2021).
[38] F. Caupin, M.A. Anisimov, Thermodynamics of supercooled and stretched water: unifying two-structure description and liquid-vapor spinodal, J. Chem. Phys. 151 (3) (2019), 034503.

[39] K.H. Kim, A. Späh, H. Pathak, F. Perakis, D. Mariedahl, K. Amann-Winkel, J. A. Sellberg, J.H. Lee, S. Kim, J. Park, K.H. Nam, T. Katayama, A. Nilsson, Maxima in the thermodynamic response and correlation functions of deeply supercooled water, Science 358 (6370) (2017) 1589–1593, https://doi.org/10.1126/science.aap8269.

[40] H. Pathak, A. Späh, N. Esmaeildoost, J.A. Sellberg, K.H. Kim, F. Perakis, K. Amann-Winkel, M. Ladd-Parada, J. Koliyadu, T.J. Lane, et al., Enhancement and maximum in the isobaric specific-heat capacity measurements of deeply supercooled water using ultrafast calorimetry, Proc. Nat. Acad. Sci. 118 (6) (2021).

[41] K.H. Kim, K. Amann-Winkel, N. Giovambattista, A. Späh, F. Perakis, H. Pathak, M. L. Parada, C. Yang, D. Mariedahl, T. Eklund, T.J. Lane, S. You, S. Jeong, M. Weston, J.H. Lee, I. Eom, M. Kim, J. Park, S.H. Chun, P.H. Poole, A. Nilsson, Experimental observation of the liquid-liquid transition in bulk supercooled water under pressure, Science 370 (6) (2020), https://doi.org/10.1126/science.abb9385.

[42] N. Giovambattista, P.H. Poole, Liquid–liquid phase transition in simulations of ultrafast heating and decompression of amorphous ice, J. Non-Crystal. Solids: X 11 (2021), 100067.

[43] J. L. F. Abascal, E. Sanz, R. G. Fernández, C. Vega, A potential model for the study of ices and amorphous water: TIP4p/ice, J. Chem. Phys. 122 (23, 2005) 234511. Doi:https://doi.org/10.1063/1.1931662.

[44] Abraham Lindahl, Van Der Spoel Hess, Gromacs 2021.3 Manual, 2021, https://doi.org/10.5281/ZENODO.5053220. https://zenodo.org/record/5053220.

[45] J.L. Finney, A. Hallbrucker, I. Kohl, A.K. Soper, D.T. Bowron, Structures of high and low density amorphous ice by neutron diffraction, Phys. Rev. Lett. 88 (2002) 225503, https://doi.org/10.1103/PhysRevLett.88.225503.

[46] R. Shi, H. Tanaka, Direct evidence in the scattering function for the coexistence of two types of local structures in liquid water, J. Am. Chem. Soc. 142 (2020) 2868–2875, pMID: 31960673, https://doi.org/10.1021/jacs.9b11211.

[47] I. Saika-Voivod, F. Sciortino, P.H. Poole, Computer simulations of liquid silica: equation of state and liquid–liquid phase transition, Phys. Rev. E 63 (1) (2000), 011202.

[48] R. Shi, H. Tanaka, Microscopic structural descriptor of liquid water, J. Chem. Phys. 148 (12, 2018) 124503.

[49] H. Tanaka, H. Tong, R. Shi, J. Russo, Revealing key structural features hidden in liquids and glasses, nature reviews, Physics 1 (2019) 333–348, https://doi.org/10.1038/s42254-019-0053-3.

[50] E.S. Loscar, C.G. Ferrara, T.S. Grigera, Spinodals and critical point using short-time dynamics for a simple model of liquid, J. Chem. Phys. 144 (13) (2016) 134501, https://doi.org/10.1063/1.4944926.

[51] E.S. Loscar, D.A. Martin, T.S. Grigera, Stability limits for the supercooled liquid and superheated crystal of lennard-jones particles, J. Chem. Phys. 147 (3) (2017), 034504.